Journal of Catalysis 266 (2009) 207–217

Contents lists available at ScienceDirect

Journal of Catalysis

journal homepage: www.elsevier.com/locate/jcat

Role of modifiers in multi-component MgO-supported Au catalysts designed for preferential CO oxidation

András Tompos [a,*], József L. Margitfalvi [b], Ervin Gy. Szabó [a], Zoltán Pászti [a], István Sajó [a], György Radnóczi [c]

[a] Institute of Nanochemistry and Catalysis, Chemical Research Center, Hungarian Academy of Sciences, 1525 Budapest, POB 17, Hungary
[b] Combitech-Nanotech Ltd. Budapest, Hungary, 1122 Budapest, Magyar jakobinusok tere 7, Hungary
[c] Institute for Technical Physics and Materials Science, Hungarian Academy of Sciences, 1525 Budapest, POB 49, Hungary

ARTICLE INFO

Article history:
Received 9 April 2009
Revised 5 June 2009
Accepted 5 June 2009
Available online 4 July 2009

Keywords:
Au/MgO
Modification of gold
PROX
High throughput experimentation

ABSTRACT

MgO-supported gold catalysts modified by V, Pb, Sm, La and Y have been investigated in order to elucidate the role of modifiers in preferential CO oxidation. All catalysts have been prepared by means of homogeneous precipitation of nitrate precursors using urea as a precipitating agent. Catalytic properties and characteristic features of catalysts were investigated in detail. Different spectroscopic techniques (XPS, FTIR and UV–Vis) and HRTEM were applied for catalyst characterization. The coverage of gold nanoparticles by small MgO clusters has been evidenced. Despite the high MgO coverage of gold, the parent Au/MgO catalysts showed high activity in CO oxidation indicating the beneficial effect of MgO in atomic closeness to Au. It has been revealed that in Pb-modified catalysts, gold has been alloyed with Pb. The results definitely indicate that Pb is responsible for the decrease in the number of gold sites involved in the activation of hydrogen. It has been shown that in multi-component catalysts MgO is decorated by nanoclusters of different metal oxides, and the Pb–Au nanoparticles are located in intimate contact to these oxides. In multi-component catalysts, the interfaces formed in this way provide new type of active site ensembles that can adsorb and activate CO and oxygen, while suppressing the activation of hydrogen.

1. Introduction

Removal of CO traces by means of catalytic oxidation from hydrogen-rich feed streams for fuel cell applications would provide a low cost technology. Vast number of studies has been devoted to the investigation of supported gold catalysts due to their superior activity in low temperature CO oxidation in comparison to other noble metal catalysts. Despite the intensive research focused on CO oxidation over gold catalysts, the nature of the active sites and working mechanism are still not clear.

First of all the stabilization of nanosized Au clusters with an average diameter of 2–5 nm is essential for attaining highly active catalysts. It has been proposed that the high activity can be attributed to (i) the formation of gold–support interface [1–5], (ii) the nonmetallic electronic properties of gold nanoclusters due to quantum-size effect [6], and (iii) the formation of step sites and strain defects [7].

Beyond the effect originated from the small particle size other factors can also be responsible for high activity. In supported gold catalysts the presence of cationic gold was proposed [8]. It was also revealed that the activity in CO oxidation is due to an ensemble of metallic Au atoms and Au cations with hydroxyl ligands [9,10]. It has been suggested that in magnesia-supported gold catalysts the activation of CO at room temperature and below requires the formation of "$(Au^{\delta+})_m$—Au_n^0" ensemble sites, in which the partially positively charged gold formed in situ is involved in the activation of CO molecule via $Au^{\delta+}$–carbonyl oxygen interaction [11]. The improved activity of Au/MgO catalysts upon the addition of modifiers such as Fe and Mn was attributed to the formation of "metal ion-gold nanocluster" ensemble sites "Me^+—Au_n^0" (Me=Fe, Mn). Above room temperature the Me^+—Au_n^0 sites have been proved to be more effective in CO activation than the parent $(Au^{\delta+})_m$—Au_n^0 ensemble sites [12]. Alternatively, anionic gold was also suggested as an active site. These species may be formed if Au is deposited on a defect-rich support, i.e., with an increased concentration of F-centres [13–15].

Whatever the type of the active site is, the results indicate that it is very sensitive to the type of support material, the presence or absence of modifiers, the method of preparation, the mode of preactivation (pretreatment) and cooling conditions used prior to the catalytic tests.

A recent review gives a summary of the most effective PROX catalysts investigated so far [16]. Different reducible oxides, such as MnO_x [17], CeO_x [18,19], FeO_x [20] and TiO_x [21], have been applied as support materials. High activity was also observed on

* Corresponding author. Fax: +36 1 4381143.
E-mail address: tompos@chemres.hu (A. Tompos).

0021-9517/$ - see front matter © 2009 Elsevier Inc. All rights reserved.
doi:10.1016/j.jcat.2009.06.007

gold supported on both basic (MgO) and refractory (SiO_2, Al_2O_3, ZrO_2) oxides [22–24]. Beneficial effect of addition of oxide modifiers ($Au/MO_x/MgO/Al_2O_3$; M=Fe, Mn) has been revealed [22,25].

Upon using Au/CeO_2 catalyst the support has been modified by various cations (Sm^{3+}, La^{3+} and Zn^{2+}) in order to obtain a defective fluorite structure with increased oxygen mobility that resulted in activity enhancement and improved resistance towards deactivation caused by the presence of CO_2 and H_2O in the PROX feed [25]. Addition of alkali (earth) metal oxides to Au/Al_2O_3 led to the stabilization of the small Au particles against sintering [26]. In the case of Au/CeO_2 systems it was shown that the synthesis route determined the strength of Au–CeO_2 interaction, which influenced the CO oxidation activity significantly [27].

Since modified Au/MgO catalysts showed stable performance under time-on-stream conditions in low temperature CO oxidation [12] our attention was focused on the investigation of these systems in PROX reaction. In our previous study a catalyst library has been designed using Au/MgO as a parent catalyst [28]. It was shown that the application of a combinatorial approach led to unexpected compositions. Pb and Sm proved to be the most effective modifiers, which have never been mentioned earlier as promoters for supported gold catalysts. It was also demonstrated that the optimization process led to different optimum compositions upon applying different pretreatment procedures prior to the catalytic test. In the simple reductive preactivation treatment exclusively hydrogen was used at 350 °C, while in combined reductive treatment an additional activation step in inert gas at 500 °C was also applied. Upon using combined reductive treatment a remarkable decrease in the gold content has been attained compared to the best composition obtained after simple reductive treatment. It has to be emphasized that after reductive treatment the best compositions did not contain vanadium, while after combined reductive treatment the V content was significant.

Because of the novelty of the compositions obtained in our previous study [28] the best catalyst compositions attained in the course of optimization using two different pretreatment procedures were further investigated using kinetic, spectroscopic and TEM methods. The behaviour of these best catalysts was compared with the behaviour of catalysts containing less components in order to elucidate the role of different modifiers.

2. Experimental

2.1. Preparation of catalysts

The catalysts were prepared parallel by means of a liquid dispensing robot in Syncore reactor (BÜCHI Labortechnik AG, Switzerland) using the rack for 24 glass reaction vessels. The following precursor compounds were used: $HAuCl_4{}^*3H_2O$ (Aldrich, 99.99%), $Pb(NO_3)_2$ (Fluka, >99%), NH_4VO_3 (Fluka, >99%), $Ba(NO_3)_2$ (Fluka, 99%), $(NH_4)_2Ce(NO_3)_2$ (Fluka, >99.0%), $Sm(NO_3)_3{}^*6H_2O$ (Aldrich, 99.9%), $AgNO_3$ (Fluka, 99%) and $Cu(NO_3)_2{}^*3H_2O$ (Fluka, 99%). First 200 mg of the MgO support (Aldrich, >99%) was loaded with different modifiers by means of the so-called homogeneous precipitation method using urea [29–31]. Water solution of the precursors (0.05 M or 0.01 M in the case of NH_4VO_3) in the required amount was dispensed and then 10 ml of 2 M urea solution in water was added followed by the addition of the support. The slurries were heated up to 100 °C and continuously shaken at 350 rpm. The slurries were vigorously boiled for 4 h to remove excess urea and to age them, followed by filtering and washing twice with deionised water. In the second step gold was added using again the urea precipitation method. Diluted solution of gold precursor (0.01 M) was mixed with 10 ml of 2 M urea solution and added to the modified supports obtained in the previous preparation step. The slurries were gradually heated up to 100 °C and maintained at this temperature for additional 4 h. The filtered and washed samples were finally dried at 60 °C. For activity tests the solids have been pressed, crushed and sieved. Catalysts with particle size between 0.200 and 0.315 mm were used in activity tests.

The designation of the catalysts exactly corresponds to their chemical composition. Additionally, catalysts prepared by applying reductive or combined reductive treatments were distinguished by "r" and "cr" endings in their denominations, respectively. As emerges from Table 1 and Table 2, the best catalyst prepared by using simple reductive treatment contains 4 w/w% Au, 3.5 w/w% Pb, 3.5 w/w% Sm, 0.6 w/w% Y, 0.6 w/w% La, and 0.0 V%, while the best catalyst prepared by applying combined reductive treatment contains 2.6 w/w% Au, 3.5 w/w% Pb, 2.4 w/w% V, 2.7 w/w% Sm, 0.0% Y, and 0.0% La with respect to MgO support. As emerges from the data given in Tables 1 and 2, the above-mentioned concentrations were maintained in all model catalysts having less number of components.

2.2. Catalytic tests

A 16-channel SS continuous-flow gas phase reactor was used as described elsewhere [32]. The amount of catalyst: 0.030 g, flow rate 30 ml/min/channel, Partial pressures in kPa: P_{CO} = 1.0 kPa, P_{O_2} = 1.0 kPa, P_{H_2} = 60 kPa, balanced with He. Kinetic studies have been performed after 24 h time-on-stream stabilization. Before testing, the catalysts were pretreated at 350 °C in hydrogen stream for 1 h in the case of simple reductive treatment, whereas in combined reductive treatment an additional 1 h pretreatment was performed at 500 °C in He atmosphere.

A quadrupole mass spectrometer (Prisma QMS 200 , Pfeiffer Vacuum Technology) was used for product analysis. If P^0_{CO} is the initial partial pressure of CO then the CO conversion in a selected channel of the combi-reactor, α^{ch}_{CO} is defined by Eq. (1):

$$\alpha^{ch}_{CO} = \frac{P^0_{CO} - P^{ch}_{CO}}{P^0_{CO}} \cdot 100, \% \quad (1)$$

where P^{ch}_{CO} is the partial pressure of CO in a selected channel of the combi-reactor. The selectivity of CO oxidation in a selected channel of the combi-reactor, S^{ch}_{CO}, is defined by Eq. (2):

$$S^{ch}_{CO} = \frac{P^0_{CO} - P^{ch}_{CO}}{2 \cdot (P^0_{O_2} - P^{ch}_{O_2})} \cdot 100, \% \quad (2)$$

where $P^0_{O_2}$ and $P^{ch}_{O_2}$ are the partial pressure of oxygen initially and after reaction in the selected channel, respectively.

If oxygen is consumed exclusively for CO oxidation, then the selectivity is 100%, whereas if no CO is reacting, the selectivity is 0. Signals of the mass spectra are supposed to be proportional to the partial pressure of different species.

Table 1
Composition of catalysts tested after reductive pretreatment.

Sample	Concentration w/w% to MgO support					
	Au	Pb	V	Y	La	Sm
Au_r	4.0	0.0	0.0	0.0	0.0	0.0
AuPb_r	4.0	3.5	0.0	0.0	0.0	0.0
AuSm_r	4.0	0.0	0.0	0.0	0.0	3.5
AuYLa_r	4.0	0.0	0.0	0.6	0.6	0.0
AuPbYLa_r	4.0	3.5	0.0	0.6	0.6	0.0
AuPbSm_r	4.0	3.5	0.0	0.0	0.0	3.5
AuYLaSm_r	4.0	0.0	0.0	0.6	0.6	3.5
AuPbYLaSm_r	4.0	3.5	0.0	0.6	0.6	3.5

Table 2
Composition of catalysts tested after combined reductive pretreatment.

Sample	Concentration w/w% to MgO support					
	Au	Pb	V	Y	La	Sm
Au_cr	2.6	0.0	0.0	0.0	0.0	0.0
AuPb_cr	2.6	3.5	0.0	0.0	0.0	0.0
AuV_cr	2.6	0.0	2.4	0.0	0.0	0.0
AuSm_cr	2.6	0.0	0.0	0.0	0.0	2.7
AuPbV_cr	2.6	3.5	2.4	0.0	0.0	0.0
AuPbSm_cr	2.6	3.5	0.0	0.0	0.0	2.7
AuVSm_cr	2.6	0.0	2.4	0.0	0.0	2.7
AuPbVSm_cr	2.6	3.5	2.4	0.0	0.0	2.7

2.3. Characterization methods

Transmission Electron Microscopy (TEM) and High-Resolution TEM investigations were carried out in order to determine particle size distribution and explore the nanoenvironment of gold particles in different modified samples, respectively. Prior to the investigations samples have been reduced at 350 °C in hydrogen for 1 h. The freshly reduced samples have been suspended in ethanol and drop dried on carbon coated copper TEM grids. TEM characterization has been executed on a Philips MORGAGNI 268D instrument, operated at 100 keV (W filament; point-resolution = 0.5 nm) while HRTEM images have been taken close to the Scherzer focus using a JEOL 3010 microscope operated at 300 kV accelerating voltage (point-resolution = 1.6 Å). Elemental mapping has been done by a Gatan TRIDIEM electron energy loss spectrometer.

X-ray diffraction patterns of catalysts reduced priory at 350 °C in hydrogen were recorded on a Philips model PW 3710-based PW 1050 Bragg–Brentano parafocusing goniometer using Cu $K\alpha$ radiation ($\lambda = 0.15418$ nm), graphite monochromator and proportional counter. The XRD scans were digitally recorded with a step size of 0.04° (2θ) and evaluated with profile fitting methods.

Infrared spectra were recorded between 4000 and 1000 cm^{-1} at room temperature using Nicolet Impact 400 FTIR instrument with 1 cm^{-1} resolution using 256 scans. As-prepared (not yet reduced) catalyst samples were ground and pressed onto self-supporting disks and were mounted in the sample holder. The "thickness" of the self-supporting disk has been considered to be proportional to the specific weight of the disk, which was about 10 mg/cm^2. The spectra were normalized to the thickness of the sample. Prior the FTIR measurements in situ thermal treatment of the sample was accomplished in a heated chamber located above the IR cell. The catalysts were reduced in flowing hydrogen (50 ml/min) at 400 °C for 1 h followed by evacuation at the same temperature for 15 min and cooling to room temperature under vacuum. First, spectrum of the sample was measured. Then 5 Torr CO was introduced into the chamber, and the spectrum was recorded again.

The diffuse reflectance UV–Vis spectra of samples reduced preliminary at 350 °C in hydrogen were collected with Jasco V-570 UV/VIS/NiR spectrophotometer equipped with an integrating sphere (type ISN 470) for the measurement of solid samples. The spectra were recorded between 200 and 800 nm, recording speed was 100 nm/min, the pitch interval was 1.0 nm, band width was 2.0 nm and resolution was 0.1 nm.

X-ray photoelectron spectroscopy (XPS) studies were carried out on an Omicron photoelectron spectrometer. The EA 125 energy analyzer was operated in the constant analyzer energy mode with pass energy of 30 eV, which resulted in acceptable resolution (around 1 eV) while maintaining high sensitivity. Spectra were taken using both Mg-$K\alpha$ and Al-$K\alpha$ X-ray sources.

Self-supporting disks of the catalyst samples were prepared similarly to those used for IR spectroscopic experiments. The disks were mounted on stainless steel sample plates.

The base pressure in the analysis chamber of the electron spectrometer is around 5×10^{-10} mbar. The system is equipped with a separate custom-designed cell in which the samples can be either pretreated or exposed to the reaction mixture at atmospheric pressure and elevated temperature. Samples can be transferred between the high-pressure cell and the analysis chamber without breaking the vacuum.

Spectra of the as-prepared samples as well as spectra after two different pretreatments were recorded. First, the as-prepared samples were analyzed without any treatment. In the subsequent pretreatment, the samples were reduced in a hydrogen atmosphere at 350 °C, while in the second pretreatment the samples have been exposed to the same reaction mixture applied in the catalytic runs (1% CO, 1% O_2, 60% H_2 and 48% He, at 80 °C for 1 h). Before analysis, the samples were evacuated in the high-pressure cell at room temperature.

Spectra have been fitted and data have been quantified by means of CasaXPS [33] and XPSMultiQuant [34] software, respectively, adopting homogeneous depth distribution model for each component. The binding energies (BEs) were referenced to the peak at 50.8 eV in the Mg 2p core level region to account for charging effects. In this case C 1s line of the hydrocarbons impurities adsorbed on the as-prepared samples appears between 285.2 and 285.5 eV, which corresponds to values generally obtained in the case of hydrocarbons adsorbed on MgO. Chemical states have been identified by means of NIST database [35].

3. Results

3.1. Catalytic tests

It has to be emphasized that the pretreatment conditions applied prior to the catalytic test strongly affected the optimal composition of multi-component Au/MgO catalysts, as it was shown in our previous work [28]. In this study the best multi-component catalysts, one obtained in reductive and another obtained in combined reductive pretreatment, have been compared to catalysts having less number of components. Catalytic results obtained over two series of catalysts are summarized in Tables 3 and 4. Prior to kinetic studies a 24 h long time-on-stream stabilization of catalysts has been accomplished.

As emerges from Table 3, in the case of catalysts tested after reductive pretreatment, the improvement of catalytic performance, such as conversion and selectivity, upon the addition of only one modifier is mainly due to the suppression of water formation, as indicated by the smaller hydrogen oxidation rate constants over modified catalysts in comparison to the parent Au/MgO catalyst (for the sake of simplicity in the AuYLa catalyst the La and Y modifiers together are considered as a single component, because of their small amount). However, the addition of a second component to the above-mentioned catalysts (see catalysts AuPbSm_r, AuPbYLa and AuYLaSm_r in Table 3) resulted in a significant increase in the rate of CO oxidation. Furthermore, selectivity values above 60% were obtained over catalysts containing lead. The best results were obtained over AuPbYLaSm_r multi-component catalyst leading to 93% conversion of CO and 62% selectivity of oxygen towards CO oxidation. In good accordance with the changes observed in the rate constants the activation energy of CO oxidation slightly decreases, while that of the water formation increases upon the addition of modifiers.

It is worth mentioning that activation energy of hydrogen oxidation always exceeds that of CO oxidation. It means that water formation is more sensitive to the temperature change than CO oxidation, therefore the increasing temperature always leads to (i) decrease of selectivity of oxygen towards CO oxidation, and

Table 3
Kinetic results over catalysts tested after reductive pretreatment.

	CO oxidation					Water formation				Conv. (%)	Sel. (%)
	k	E_a (kJ/mol)	ln(A)	n_{CO}	n_{O_2}	k	E_a (kJ/mol)	ln(A)	n_{O_2}		
Au_r	13.7	27	12	0.4	0.3	6.6	39	15	0.5	73	47
AuPb_r	13.2	27	12	0.4	0.4	2.4	44	16	0.6	71	57
AuSm_r	12.5	19	9	0.4	0.4	1.7	40	14	0.5	68	64
AuYLa_r	11.3	22	10	0.4	0.3	3.4	46	17	0.5	68	56
AuPbSm_r	19.0	14	8	0.6	0.3	1.4	57	20	0.4	90	67
AuPbYLa_r	15.0	24	11	0.6	0.3	2.0	57	20	0.5	86	65
AuYLaSm_r	15.9	24	11	0.5	0.4	4.2	51	19	0.5	83	55
AuPbYLaSm_r	20.6	21	10	0.5	0.2	3.8	51	19	0.5	93	62

k – Rate constant; E_a – activation energy; A – pre-exponential factor; n_{CO} and n_{O_2} – the reaction orders for CO and O_2, respectively. W_{cat} = 30 mg; conditions applied for the determination of conversion of CO as well as selectivity of oxygen towards CO oxidation: T = 80 °C; F = 30 ml/min, P_{CO} = 1.0 kPa; P_{O_2} = 1.0 kPa; P_{H_2} = 600 kPa; He balance. Conditions applied for the determination of rate constants and reaction orders: T = 80 °C; F = 50, 60, 75, 100 ml/min; P_{CO} = 0.7, 1.0, 1.4, 2.0 kPa; P_{O_2} = 1.0, 1.4, 1.7, 2.0 kPa; P_{H_2} = 600 kPa; He balance. For the determination of activation energy the reaction temperature has been changed; T = 30, 45, 60, 80 °C; F = 50, 60, 75, 100 ml/min; P_{CO} = 1.0 kPa; P_{O_2} = 1.0 kPa; P_{H_2} = 600 kPa; He balance.

Table 4
Kinetic results over catalysts tested after combined reductive pretreatment.

	CO oxidation					Water formation				Conv. (%)	Sel. (%)
	k	E_a (kJ/mol)	ln(A)	n_{CO}	n_{O_2}	k	E_a (kJ/mol)	ln(A)	n_{O_2}		
Au_cr	4.7	27	11	0.5	0.3	1.6	34	12	0.6	36	62
AuPb_cr	6.9	27	11	0.5	0.2	1.7	35	13	0.5	57	71
AuV_cr	4.0	26	10	0.4	0.3	2.1	37	13	0.5	38	56
AuSm_cr	5.6	21	9	0.4	0.4	2.0	37	13	0.5	46	62
AuPbV_cr	9.3	25	11	0.4	0.3	2.8	29	11	0.4	68	63
AuPbSm_cr	8.1	19	9	0.5	0.4	1.8	34	12	0.5	63	72
AuVSm_cr	17.4	25	11	0.4	0.4	11.7	43	17	0.5	73	41
AuPbVSm_cr	19.5	23	11	0.4	0.3	6.5	50	19	0.5	92	55

(ii) a maximum in CO conversion, which is in good accordance with our earlier results [28].

In the case of catalysts tested after combined reductive treatment the addition of modifiers increases both the rate of CO and hydrogen oxidation reactions. The only exception is the V; over the bimetallic AuV_cr catalyst the CO oxidation activity is slightly decreased at 80 °C. It has to be emphasized that the overall activity of the parent Au_cr catalyst is much lower than that of the Au_r. This low activity can probably be attributed to the lower Au content.

Results given in Table 4 show a pronounced positive synergism between the V and Sm. Simultaneous presence of these two modifiers increases significantly both rate constants. Further addition of Pb to the AuVSm_cr system results in further improvement of conversion and selectivity, which is due to the smaller water formation rate constant upon the addition of Pb (compare AuVSm_cr to AuPbVSm_cr in Table 4).

It has to be mentioned that there is an apparent contradiction between the high activity of the AuVSm_cr in the hydrogen oxidation and its higher activation energy in comparison to the unmodified catalyst. It is only possible if the pre-exponential factor in the Arrhenius correlation for water formation increases significantly and over-compensates the decrease of the exponential factor. As emerges from Table 4 the ln(A) is significantly higher in the case of the AuSmV_cr three-component system than in the case of the unmodified gold catalyst. The pre-exponential factor is the so-called "frequency" factor that correlates to the total number of collisions between the reactants in unit time. Therefore, as the initial concentration of O_2 and H_2 was the same in the feed gas when comparing modified and unmodified catalysts, the addition of V and Sm together can (i) either increase the amount of gold exposed to the surface, (ii) or modify the nanoenvironment of gold in such a way that the new SmV–Au interface has higher affinity towards reactants than the parent gold–MgO itself. In this respect it is suggested that over the new active sites the surface concentration of oxygen is higher than over the unmodified gold catalyst.

It is also interesting that the pre-exponential factor of water formation obtained over the unmodified Au_r catalyst also exceeds significantly that of water formation obtained over the unmodified Au_cr catalyst (compare ln(A) = 15 and ln(A) = 12 in Tables 3 and 4, respectively). The only difference between these catalysts is the gold content. The higher gold content evidently leads to a higher amount of surface gold exposed to the gas phase.

Investigation of reaction orders determined for CO and O_2 in the two competitive reactions showed that there is no significant change in reaction mechanism upon the addition of modifiers either after reductive or combined reductive pretreatment. In CO oxidation the reaction order for CO and O_2 is roughly 0.4 and 0.3, respectively, while in water formation the reaction order for O_2 is ca. 0.5 regardless of the catalyst composition or pretreatment conditions applied.

3.2. TEM and HRTEM characterization

The particle size distributions of gold over parent and modified Au_r catalysts are shown in Fig. 1. The results show that the average particle size increases slightly upon the addition of modifiers. A similar trend has been found when Au_cr and its modified versions were investigated.

HRTEM images of the unmodified catalyst (Au_r) can be seen in Fig. 2. The spacing of the fringes visible in these crystallites was found to be equal to 2.14 Å, which can be identified as MgO (200) fringes (ICDD JCPDS card 45-0946). Superposition of reflections from crystallographic planes of MgO in different orientations can be discovered on the photograph indicating that MgO crystallites overlap each other. Images of individual crystallites can be re-

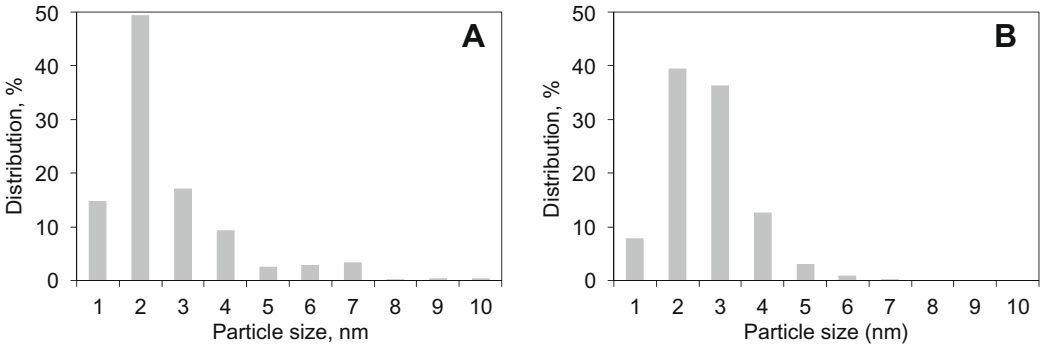

Fig. 1. Particle size distribution of gold in Au_r and AuPbYLaSm_r catalysts (A and B).

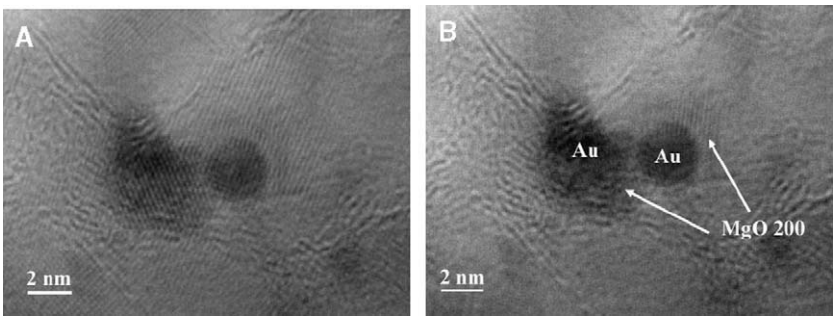

Fig. 2. HRTEM images of the Au_r catalyst before and after using the inverse Fourier filtering technique (A and B).

moved separately using the Fourier filtering technique. As emerges from Fig. 2B, after removal of the larger MgO crystallites digitally, nanosized crystalline particles attached to gold nanoparticles remain still visible. Consequently, nanosized crystalline magnesia is found in the atomic closeness to the gold particles. This finding indicates that the surface or edges of gold are partially covered by nanosized magnesia. The HRTEM image in Fig. 2 reveals rounded gold particles with unclear contours. The spherical shape of the particles indicates that the surface of gold nanoparticles is covered by MgO, leading to the disappearance of surface anisotropy of Au.

It has to be emphasized that the Au_r catalysts have been prepared by means of homogeneous precipitation method. In Fig. 3A a HRTEM image of a gold nanocluster over Au/MgO catalyst is shown which was prepared by means of traditional heterogeneous precipitation. In this image clear contours of a gold nanoparticle can be seen, consequently in Au/MgO catalyst prepared by heterogeneous precipitation the gold nanocluster is not covered by magnesia. It is interesting that in this image the fringes of gold (1 1 1) coincide with those of the MgO (1 1 1) indicating the same 2.37 Å spacing in the two crystallites corresponding to both MgO (1 1 1) and Au (1 1 1). This finding is supported further by Fig. 3B, which shows the FFT image of Fig. 3A where only one reflection can be detected. The tabulated spacing for Au (1 1 1) and MgO (1 1 1) is 2.36 Å and 2.43 Å, respectively.

Characteristic photographs of different multi-component systems are shown in Fig. 4. In Fig. 4A rounded edges of gold nanoparticle of the three-component AuPbSm_r are conspicuous providing further evidence for covering Au nanoclusters by MgO. Furthermore, as emerges from Fig. 4A gold is located in the atomic closeness of Sm_2O_3 crystallites. Sm_2O_3 (2 2 2) surface of the cubic unit cell has been identified by its 3.14 Å d-spacing (ICDD JCPDS card 15-0813). It is interesting that the spacing of Au (1 1 1) fringes in Fig. 4 (2.43 Å) exceeds that of given in the related art (2.36 Å). The larger lattice spacing could also be observed in several Au crystallites of the AuPbSm_r catalyst. It clearly indicates that Pb is dissolved in the Au nanoparticles and the alloying leads to an expansion of the unit cell of gold. This can correspond to 5–10 at% of dissolved Pb in Au according to the Vegards law [36].

In Fig. 4B showing a HRTEM image of AuVSm_cr catalyst an extended V_2O_5 crystallite is visible. The lattice fringe spacing was found to be equal to 3.4 Å, which is likely due to V_2O_5 (1 0 1) (ICDD JCPDS card 72-0133). The darker areas correspond to small Au nanoparticles; however, the corresponding fringes are not visible

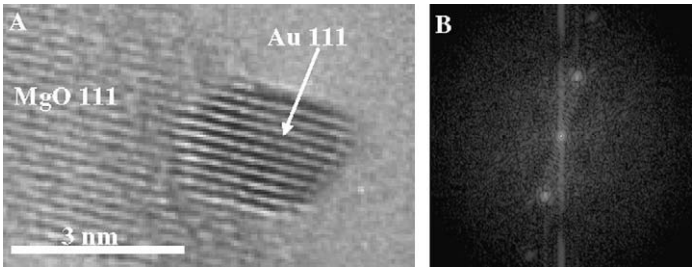

Fig. 3. HRTEM image of a Au/MgO catalyst prepared by heterogeneous precipitation and its transformation by means of the Fourier filtering technique (A and B).

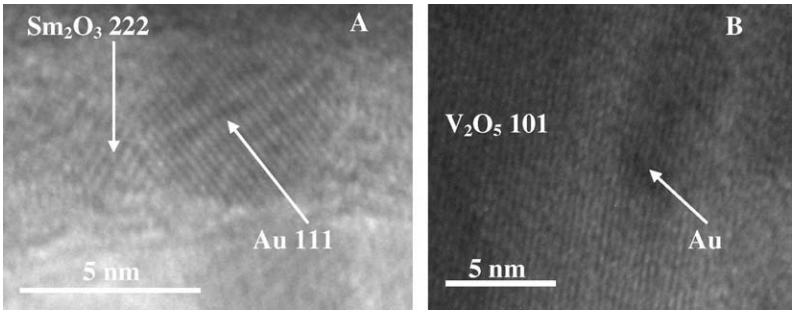

Fig. 4. HRTEM image of AuPbSm_r and AuVSm_cr catalysts (A and B).

in this image. Consequently, based on this finding the atomic closeness of V_2O_5 to Au is clearly demonstrated.

Although the microscope has been equipped with an EELS facility in order to map different modifiers, the surface concentration of modifiers was too low and the modifiers introduced to the MgO support were too dispersed for achieving convincing results especially about local coexistence of modifiers.

3.3. XRD characterization

According to XRD spectra shown in Fig. 5 crystalline gold has been identified both in the parent and the modified samples. In the multi-component catalysts besides Au only MgO crystallites have been detected. This finding indicates that the modifiers are present in too small amounts to be visible by XRD as well as they are in highly dispersed form.

It has been revealed that gold is more crystalline in unmodified Au_r catalyst than in AuPbYLaSm_r. Despite the same gold content of these catalysts (see Table 1) more intensive diffraction peak of Au is visible on the XRD spectra of the Au_r (see Fig. 5). Consequently, the addition of modifiers results in lower crystallinity. This finding can be explained as follows: (i) decrease of the particles size in modified catalysts, or (ii) gold is diluted by different modifiers. In both cases the long-range order of Au crystallites is ceased.

Catalysts containing both Sm and V show very unique behaviour. Fig. 6 shows the XRD spectrum of the AuVSm_cr catalyst after reductive and combined reductive treatment, respectively. The XRD pattern suggests that (i) $SmVO_4$ is crystalline and (ii) forms relatively large crystallites on the surface of MgO. As emerges from Fig. 6 the reflections attributed to $SmVO_4$ are slightly more intensive after combined reductive treatment. Fig. 6 also shows that the combined reductive treatment, i.e., pretreatment in argon at elevated temperature (500 °C) increases also the crystallinity of MgO support.

3.4. XPS characterization

Summary of XPS results obtained over Au_cr and AuPbVSm_cr under different conditions can be seen in Tables 5–7. It has to be emphasized that data were successfully reproduced using two different X-ray sources mentioned in the experimental part.

According to Table 5 it has been evidenced that before any treatment the support mainly consists of $Mg(OH)_2$, which is indicated by the binding energy of the main peak in O 1s core level region (531.2–531.5 eV [37–39]). Additionally, the surface concentration ratio of O to Mg equals to ca. 2. The peak at around 290.3 eV in the C 1s region reveals the presence of $Mg(CO_3)_2$ as well. The C 1s peak centred at ca. 285.0 eV is due to adsorbed hydrocarbons. Initially the catalysts contain gold in the salt form (Au $4f_{7/2}$ binding energy around or above 86.0 eV). During data collection gradual reduction is observable, which is evidenced by a growing peak around 85.0 eV. This binding energy - which is still high for bulk metallic gold – can be explained by the generally observed size-dependent core level shift reported for metal nanoparticles [40,41]. In general, the modifiers are present in oxidized forms, although the analysis of vanadium is quite ambiguous as its $2p_{3/2-1/2}$ doublet that could be detected with the highest intensity, coincides with the satellite region of the strong O 1s line.

Results after pretreatment are summarized in Table 6. The formation of MgO was revealed, since the main component in O 1s region was the peak centred at ca. 530 eV, which can be ascribed to O^{2-} of MgO [35]. Moreover, the surface ratio of Mg to O is close to 1 (see Table 6). The higher binding energy O 1s component at 532.4 eV is due to hydroxyl groups on the oxide surface. It is interesting that in spite of the high temperature

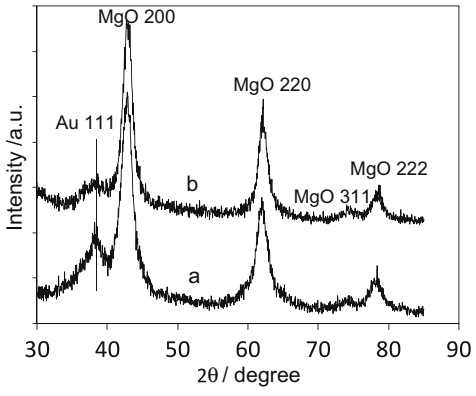

Fig. 5. XRD spectrum of catalysts: (a) Au_r, and (b) AuPbYLaSm_r.

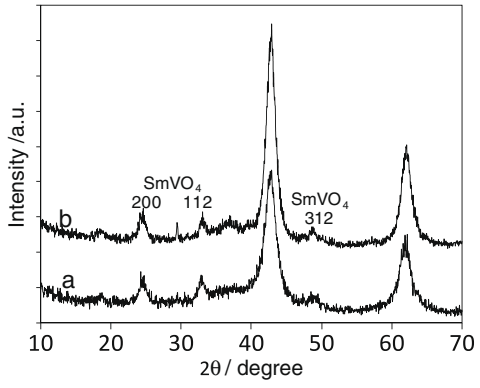

Fig. 6. XRD spectrum of catalyst AuVSm_cr after (a) simple reductive treatment, and (b) combined reductive pretreatment.

pretreatment carbonates as well as hydrocarbons are still in large amounts on the surface. There was no remarkable change in the state of gold; it is present in the form of reduced nanoparticles. However, the evaluation of XP spectra of the four-component AuPbVSm_cr catalyst in the Pb 4f core level region shows that upon pretreatment the Pb is reduced to a large extent. This finding is also demonstrated on the spectra shown in Fig. 7A. As emerges from Fig. 7A after pretreatment the main component of the Pb 4f doublet shifts considerably towards lower binding energies, reaching values characteristic for metallic Pb (Pb $4f_{7/2}$ line at 136.6 eV [35]). It is only possible if lead is in the atomic vicinity to gold nanoclusters, as direct reduction of PbO_x with hydrogen is not presumable. This statement has been proved experimentally. MgO-supported mixed oxide powder containing Pb, V and Sm only has been prepared and investigated by means of XP spectroscopy. In Fig. 7B it is clearly evidenced that after pretreatment, in the absence of Au, no reduction of PbO_x was observed. In the AuPbVSm_cr catalyst upon pretreatment the other modifiers, such as Sm and V, did not show detectable changes with respect to the untreated catalyst.

Table 7 shows XPS results obtained after PROX reaction. Pb can be detected in oxidized form again (Pb $4f_{7/2}$ line at 138.2 eV), while the other components remain unchanged in comparison to the states after pretreatment. The PROX reaction had a significant effect on surface gold content of Au_cr catalyst: amount of the gold detected on the surface was significantly smaller after the PROX reaction than before, which can be attributed to some morphological changes upon reaction. Sintering upon reaction can lead to larger particles and thus decreased surface concentration of gold. In contrast to this the AuPbVSm_cr four-component system showed increased morphological stability; no decline in the gold signal was observed upon PROX reaction. It can be con-

Table 5
XPS data of catalysts before any treatment.

Catalyst		Au $4f_{7/2}$	Pb $4f_{7/2}$	V $2p_{3/2}$	Sm $3d_{5/2}$	Mg 2s, 2p	O 1s	C 1s
Au_cr	Conc. (at%)	0.3–0.4	–	–	–	26	58	16
	State	Partly reduced (86.5–85.5)				$Mg(OH)_2$ (89.5 – 2s) (50.8 – 2p)	$Mg(OH)_2$ (531.5)	CO_3^{2-} (290.6) and HCs (285.2)
AuPbVSm_cr	Conc. (at%)	0.2	0.3	0.8	0.3	23	56	19
	State	Partly reduced (85.7–84.7)	Oxidized (138.4)	Slightly reduced (516)	Sm_2O_3(1082.0)	$Mg(OH)_2$ (89.5 – 2s) (50.8 – 2p)	$Mg(OH)_2$(531.2)	CO_3^{2-} (290.0) and HCs (285.0)

Binding energies (eV) are in parentheses.

Table 6
XPS data of catalysts after pretreatment.

Catalyst		Au $4f_{7/2}$	Pb $4f_{7/2}$	V $2p_{3/2}$	Sm $3d_{5/2}$	Mg 2s, 2p	O 1s	C 1s
Au_cr	Conc. (at%)	0.4	–	–	–	43	47	10
	State	Reduced (85.0)				MgO (89.6 – 2s) (50.8 – 2p)	MgO (530.1) hydroxyl (532.1)	CO_3^{2-} (290.3) and HCs (285.7)
AuPbVSm_cr	Conc. (at%)	0.2	0.3	0.6	0.5	41	49	8
	State	Reduced (84.8)	Metallic (136.6) and oxidized (138.9)	Slightly reduced (516)	Sm_2O_3(1082.0)	MgO (89.5 – 2s) (50.8 – 2p)	MgO (530.2) hydroxyl (532.4)	CO_3^{2-} (290.2) and HCs (285.5)

Binding energies (eV) are in parentheses.

Table 7
XPS data of catalysts after PROX reaction.

Catalyst		Au $4f_{7/2}$	Pb $4f_{7/2}$	V $2p_{3/2}$	Sm $3d_{5/2}$	Mg 2s, 2p	O 1s	C 1s
Au_cr	Conc. (at%)	0.25	–	–	–	47	46	7
	State	Reduced (85.0)				MgO (89.6 – 2s) (50.8 – 2p)	MgO (530.0) hydroxyl (532.1)	CO_3^{2-} (290.4) and HCs (286.0)
AuPbVSm_cr	Conc. (at%)	0.2	0.3	0.9	0.3	42	48	8
	State	Reduced (85.0)	Oxidized (138.2)	V_2O_5 (517)	Sm_2O_3 (1081.8)	MgO (89.5 – 2s) (50.8 – 2p)	MgO (530.3) hydroxyl (532.4)	CO_3^{2-} (290.1) and HCs (285.8)

Binding energies (eV) are in parentheses.

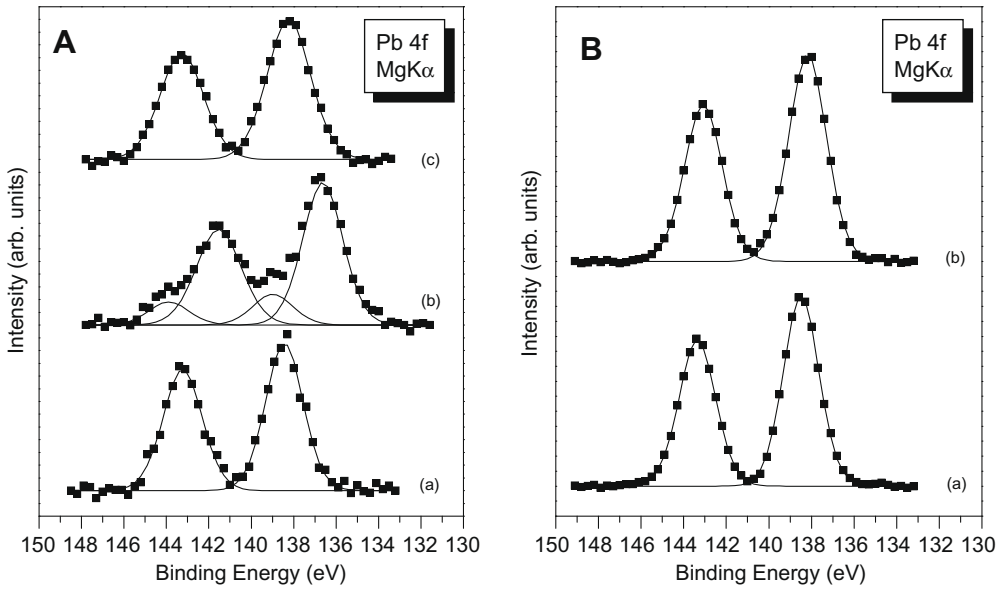

Fig. 7. X-ray photoelectron spectra in the Pb 4f core level region of catalyst AuPbVSm_cr and PbVSm/MgO (A and B): (a) before treatments, (b) after pretreatment, and (c) after PROX reaction. Experimental points are shown by rectangles while continuous lines represent the fitted $4f_{7/2}$ and $4f_{5/2}$ components.

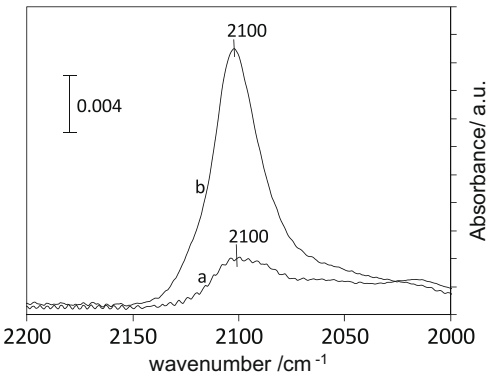

Fig. 8. FTIR spectra of CO adsorption over unmodified gold catalysts supported on MgO prepared by (a) homogeneous, and (b) heterogeneous precipitation (P_{CO} = 5 Torr; T = RT).

cluded that the modifiers have a strong stabilization effect on Au nanoparticles.

3.5. FTIR characterization

Infrared spectra of CO adsorbed on supported gold catalysts usually give an intensive absorption band around 2100 cm^{-1} [42]. Fig. 8 shows infrared spectra of CO adsorbed on magnesia-supported gold catalysts prepared in different ways. Catalyst prepared by homogeneous precipitation had only a very weak CO absorption band, while catalyst with a similar gold content prepared by heterogeneous precipitation showed a very intensive band. It was supposed that the homogeneous precipitation technique applied is responsible for the suppressed CO adsorption. A possible explanation for the suppression of CO adsorption over catalyst prepared by homogeneous precipitation can be the deposition of MgO crystallites onto the gold crystallites during the preparation. It is presumable that during the preparation magnesia is dissolved partially under condition of boiling and after the precipitation step when the slurry is cooled down to RT, crystallization of MgO takes place. As the solubility of MgO is higher than that of gold hydroxides, upon cooling first gold containing precipitates and surface complexes appear, which are then covered by magnesia nanoparticles.

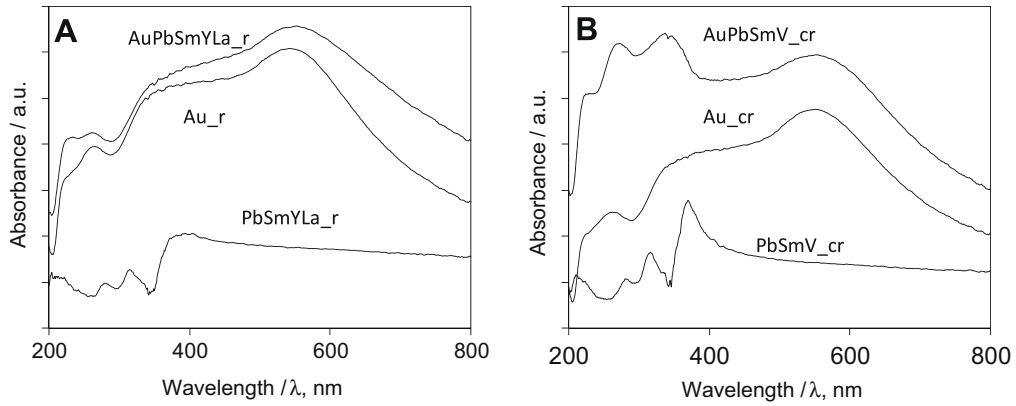

Fig. 9. UV spectra of catalysts after reductive and combined reductive pretreatment (A and B).

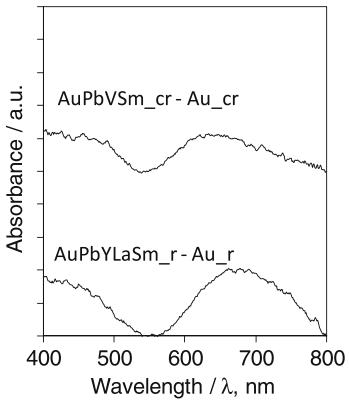

Fig. 10. Difference UV spectra of multi-component catalysts and unmodified catalysts after reductive and combined reductive pretreatment.

3.6. UV–Vis characterization

The UV spectra of the two best multi-component catalysts obtained after the applied reductive and combined pretreatments can be seen in Fig. 9. The spectra are compared to those of unmodified Au catalysts and to those of multi-component samples prepared without gold. A pronounced maximum in 500–550 nm wavelength region appears over gold containing samples that can be ascribed to plasmon resonance of conduction electrons of metallic gold particles as a response to optical excitation [43]. It has to be mentioned that neither the modifiers nor the magnesia has absorption in this region (see Fig. 9).

In order to see the effect of modifiers on the plasmon resonance of gold particles spectra of unmodified catalysts have been subtracted from those of the modified catalysts (see Fig. 10). At 550 nm a minimum appears indicating that in the original, un-subtracted spectra of the modified catalysts the plasmon resonance is less pronounced than in the spectra of the unmodified catalysts. This finding indicates indirectly that gold nanoparticles are either smaller or diluted by additives in the modified samples. In both cases the electronic structure of the Au nanoparticles is changed that modifies the plasmon resonance of the conduction electrons.

4. Discussion

In this study kinetic, spectroscopic and TEM results were obtained with the aim to elucidate the increased activity and selectivity of multi-component Au/MgO catalysts in the PROX reaction. In order to understand why and how different modifiers act in multi-component MgO-supported gold catalyst the above-mentioned kinetic and characterization results, complementing each other, will be discussed.

4.1. MgO coverage of the surface

In one of our previous studies it was clearly shown that MgO has a positive effect on the activity of Al_2O_3 supported gold catalysts in CO oxidation [44]. In the present study MgO has been used as a support. It was supposed that the support itself had a significant role in the PROX reaction. Interestingly, on the bases of the characterization results a quite unexpected phenomenon was figured out, namely the surface of the catalyst is partially covered by MgO. In this respect the advantage of homogeneous precipitation used for the preparation is questionable to the traditional heterogeneous precipitation technique. Theoretically, in homogeneous precipitation, decomposition of urea at increasing temperature results in the gradual increase of pH homogeneously distributed in the solution, which leads to uniform size of nanoparticles. Additionally, the synthesis is a simple one-pot method that holds the promise of high reproducibility. Nevertheless, the dissolution of MgO support in the meantime and the crystallization of $Mg(OH)_2$ over the precipitated Au particles means a strong drawback to heterogeneous precipitation, which decreases the exposed surface of gold nanoparticles significantly. Only little CO absorption over the Au surface is detectable by means of FTIR (Fig. 8). However, despite the suppressed CO adsorption the CO oxidation activity of multi-component catalysts prepared by means of homogeneous precipitation is excellent (Tables 3 and 4). From kinetic point of view the weak adsorption strength results in low residence time of CO on the surface. In order to compensate the low residence time of CO significantly higher turnover frequency is required over the active sites of catalysts prepared by homogeneous in comparison to heterogeneous precipitation. It is supposed that the MgO support can activate oxygen, which compensates the decreased surface concentration of CO. The atomic contact between the gold nanoparticles and MgO has been evidenced in HRTEM images shown in Fig. 2, which makes possible fast reaction between activated oxygen and CO.

4.2. Role of metal-oxide modifiers

Based on the characterization results most of the modifiers added to the parent Au/MgO catalyst are in the form of oxides. However, different optimum combinations of oxides were found for catalysts tested after reductive and combined reductive treatment (Sm, Y, La and V, Sm, respectively). Besides, both series of catalysts contain Pb, which, however, is partially reduced and is present in a metallic form after submission to different pretreatments prior to catalytic tests.

In the case of "r" series of catalysts the addition of Sm (AuSm_r) or Y and La (AuYLa_r) oxides as modifiers resulted in a significant improvement in the selectivity values (see Table 3), while the activity remained almost unchanged. The introduction of Sm to the above-mentioned catalyst resulted in significant activity improvement, while maintaining the increased range of selectivity (AuYLaSm_r).

The performance of the parent catalyst after combined reductive treatment is much lower than that after simple reductive treatment. This fact is attributed to the lower Au content as it was discussed earlier (see Table 4). Upon the introduction of Sm pronounced improvement in the overall performance was observed while in the case of modification by V the activity remained unchanged, but the selectivity decreased. The simultaneous addition of Sm and V (AuVSm_cr catalyst) resulted in a remarkable synergetic effect (see the activity increase in both competitive reactions in Table 4).

It has to be emphasized that the best multi-component catalysts (AuPbYLaSm_r and AuPbVSm_cr) were obtained upon two separate optimizations using reductive and combined reductive pretreatments prior to catalytic tests [28]. In the course of optimizations, the most appropriate components have been selected through iterative processes. Despite the same potential modifiers applied in the two experimental spaces there are significant differences in the resulted two optima. Synergistic effect of Sm and V prevails exclusively after combined reductive pretreatment (in catalyst AuPbVSm_cr) while in the other optimum composition (AuPbYLaSm_r) there is no V at all. These phenomena have to be elucidated.

In the co-precipitation of NH_4VO_3 and $Sm(NO_3)_3$ on the MgO support formation of $SmVO_4$ was directly evidenced on XRD spectra shown in Fig. 6. However, crystalline $SmVO_4$ could be detected after both pretreatments. Thus, the formation of $SmVO_4$ is not the single factor that is responsible for the increased activity in PROX

reactions over catalysts submitted to combined reductive pretreatment.

As emerges from Table 6 after combined pretreatment slightly reduced vanadia species (VO_x) can be detected, i.e., coexistence of V^{5+} and V^{4+} is supposed on the surface of AuPbVSm_cr catalyst. In this catalyst V is about in a three-time excess to Sm in atomic ratio. The presence of significant amount of free VO_x is also very probable, which has a remarkable surface mobility above a given temperature. The surface mobility of VO_x solid molecules begins at its Tamman temperature (340 °C) [45]. Taking into account the temperature at which the catalysts were pretreated upon combined reductive treatment (500 °C), it can be inferred that there was a great VO_x mobility during this process. High mobility of VO_x and the strong driving force of the MgO–$SmVO_4$ mixed oxide system to lower its surface free energy [46] can lead to the formation of a layer of surface vanadium species. This assumption is supported by Fig. 4B showing an extended V_2O_5 crystallite on the AuVSm_cr catalyst.

It was found that the reducibility of surface V^{5+} species increased in the presence of $SmVO_4$ [46]. The increased reducibility facilitated selective oxidative dehydrogenation of propane to propene through a redox type (Mars Van Krevelen) mechanism over $SmVO_4$ impregnated catalysts [46]. Analogously, a similar synergism between $SmVO_4$ and surface VO_x species can be supposed over MgO-supported catalyst in PROX as well.

On the basis of kinetic results it was postulated that in multi-component catalysts the presence of Sm and V modifiers can increase the surface concentration of oxygen during the PROX process, since the pre-exponential factor in water formation reaction increased remarkably in comparison to the corresponding value obtained over the unmodified catalyst. Actually, the apparent higher surface concentration of oxygen over multi-component catalysts in comparison to the unmodified gold catalyst can be due to the easier reducibility of V^{5+} species and thus higher surface mobility of oxygen species over new type of active sites. The new type of active sites consists of a VO_x layer over $SmVO_4$ and MgO and interfaces of these species with Au nanoparticles. After a simple reductive pretreatment formation of the VO_x layer would be less probable. The applied low temperature in simple reductive pretreatment (350 °C) would not result in high surface mobility and thus spreading of VO_x over the surface.

In catalysts submitted to simple reductive treatment there is also an increase in the pre-exponential factor in comparison to the unmodified catalyst (Table 3), whose enhancement is, however, not as pronounced as in catalysts submitted to combined reductive treatment (Table 4). Oxides of Sm, Y and La can facilitate easier adsorption of oxygen from the gas phase and thus result in higher oxygen concentration on the surface of the catalyst. The increased surface oxygen concentration, however, cannot compensate the increase of the activation energy in water formation reaction; therefore the reaction rate of hydrogen oxidation decreases.

Irrespective of the pretreatment used atomic closeness of different oxides to Au in MgO-supported Au catalysts makes possible the formation of metal ion – gold nanocluster ensemble sites ("Me^{n+}–Au^0"), which are supposed to be responsible for the activation of CO [12]. Additionally, XP spectra indicated that the metal-oxide modifiers can stabilize small particle size of gold nanoclusters.

4.3. Role of Pb

All catalysts with the highest CO selectivity contained lead irrespective of the pretreatment conditions applied. The addition of lead to AuYLaSm_r or to AuVSm_cr catalysts resulted in a pronounced increase both in the activity and selectivity. In these two catalysts the rate of CO oxidation has the highest values (see Tables 3 and 4).

Both direct and indirect characterization evidences are available supporting dissolution of Pb into gold nanoparticles. Dilution of gold by Pb results in larger particle size (Fig. 1) as well as smaller crystallinity (Fig. 5). Reduction of Pb was evidenced by means of XP spectra (Fig. 7A). Atomic closeness of Pb to Au is prerequisite for direct reduction of Pb by hydrogen. The wider lattice fringes of Au in HRTEM image (Fig. 4A) and lower intensity of the plasmon resonance on UV–Vis spectra (Fig. 9) also indicate that gold nanoclusters are diluted by Pb.

It is very probable that hydrogen adsorption over AuPb alloys is strongly suppressed in comparison to monometallic Au catalysts. Suppression of hydrogen adsorption results in higher selectivity in PROX reaction as the probability of hydrogen oxidation is decreased. Addition of Pb always resulted in smaller water formation reaction rate constant (see Tables 3 and 4).

5. Conclusions

The results indicate that in preferential CO oxidation the nanoenvironment of gold has a strong impact on both the activity and selectivity. Experimental evidences were collected indicating that the nanoenvironment of gold is determined not only by the composition of the catalysts, but also by the pretreatment method applied prior to the catalytic tests. On the bases of results discussed in this study two different models shown in Fig. 11 can be envisaged representing the schematic structures of multi-component catalysts.

In both types of multi-component Au/MgO catalysts, Pb and Sm have a decisive contribution to the overall performance. The positive influence of lead is due to its ability to form alloy with gold. In this way both the enhanced activity and selectivity in PROX reaction are due to the suppression of hydrogen activation.

The enhancement of pre-exponential factors in water formation reaction upon the addition of oxide modifiers indicates that the different metal oxide modifiers provide favourable adsorption sites for oxygen thus enhancing the surface oxygen concentration. Due to the atomic contact between oxide modifiers and gold the formation of metal ion – gold nanocluster ensemble sites has a strong contribution to the activation of CO over the multi-component catalyst obtained after simple reductive pretreatment.

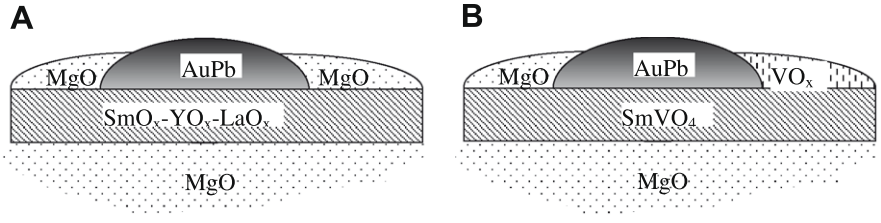

Fig. 11. Nanoenvironment of gold particles in multi-component catalyst obtained after simple reductive and combined reductive pretreatments (A and B).

It was proved that the combined reductive treatment facilitated spreading of vanadium species over the surface and resulted in VO_x layer over $SmVO_4$ and MgO in close atomic contact to Au (Fig. 11B). In the multi-component catalyst obtained upon combined reductive treatment, similarly to the catalyst obtained after simple reductive treatment, the synergism between different components in atomic closeness to Au is one of the key factors in determination of PROX activity. Additionally, modifiers have a strong stabilization effect on Au nanoparticles.

It has to be emphasized that MgO support itself has a pronounced effect on performance of catalysts in PROX reaction. Due to the homogeneous precipitation technique used for preparation, the gold nanoparticles are partially covered by MgO. However, negative effect of the MgO coverage is over-compensated by the increase in the CO oxidation activity due to the atomic closeness between MgO nano-crystallites and Au nanoparticles. HRTEM results indicate that the high temperature treatment of modified catalysts in argon increases the crystallinity of both MgO and nanosized mixed oxides.

Acknowledgment

Partial financial support by OTKA (Grant F 049742 to A.T.) is greatly acknowledged.

References

[1] M. Haruta, S. Tsubota, T. Kobayashi, H. Kageyama, M.J. Genet, B. Delmon, J. Catal. 144 (1993) 175.
[2] S.D. Lin, M. Bollinger, M.A. Vannice, Catal. Lett. 17 (1993) 245.
[3] M. Bollinger, M.A. Vannice, Appl. Catal. B: Environ. 8 (1996) 417.
[4] F. Boccuzzi, A. Chiorino, M. Manzoli, P. Lu, T. Akita, S. Ichikawa, M. Haruta, J. Catal. 202 (2001) 256.
[5] R.J.H. Grisel, C.J. Weststrate, A. Goossens, M.W.J. Craje, A.M. van der Kraan, B.E. Nieuwenhuys, Catal. Today 72 (2002) 123.
[6] M. Valden, X. Lai, D.W. Goodman, Science 281 (1998) 1647.
[7] M. Mavrikakis, P. Stoltze, J.K. Norskov, Catal. Lett. 64 (2000) 101.
[8] N.A. Hodge, C.J. Kiely, R. Whyman, M.R.H. Siddiqui, G.J. Hutchings, Q.A. Pankhurst, F.E. Wagner, R.R. Rajaram, S.E. Golunski, Catal. Today 72 (2002) 133.
[9] G.C. Bond, D.T. Thompson, Gold Bull. 33 (2000) 41.
[10] C.K. Costello, M.C. Kung, S.-O. Oh, Y. Wang, H.H. Kung, Appl. Catal. A: Gen. 232 (2002) 159.
[11] J.L. Margitfalvi, A. Fási, M. Hegedűs, F. Lónyi, S. Gőbölös, N. Bogdanchikova, Catal. Today 72 (2002) 157.
[12] J.L. Margitfalvi, M. Hegedűs, Á. Szegedi, I. Sajó, Appl. Catal. A: Gen. 272 (2004) 87.
[13] W.T. Wallace, R.L. Whetten, J. Am. Chem. Soc. 124 (2002) 7499.
[14] L.D. Socaciu, J. Hagen, T.M. Bernhardt, L. Woste, U. Heiz, H. Hakkinen, U. Landman, J. Am. Chem. Soc. 125 (2003) 10437.
[15] H. Hakkinen, U. Landman, J. Am. Chem. Soc. 123 (2001) 9704.
[16] E.D. Park, D. Lee, H.C. Lee, Catal. Today 139 (2009) 280.
[17] R.M.T. Sanchez, A. Ueda, K. Tanaka, M. Haruta, J. Catal. 168 (1997) 125.
[18] S. Carrettin, P. Concepcion, A. Corma, J.M.L. Nieto, V.F. Puntes, Angew. Chem. Int. Ed. 43 (2004) 2538.
[19] F. Arena, P. Famulari, G. Trunfio, G. Bonura, F. Frusteri, L. Spadaro, Appl. Catal. B: Environ. 66 (2006) 81.
[20] M.J. Kahlich, H.A. Gasteiger, R.J. Behm, J. Catal. 182 (1999) 430.
[21] J. Steyn, G. Pattrick, M.S. Scurrell, D. Hildebrandt, M.C. Raphulu, E. van der Lingen, Catal. Today 122 (2007) 254.
[22] R.J.H. Griesel, B.E. Nieuwenhuys, J. Catal. 199 (2001) 48.
[23] H.-S. Oh, J.H. Yang, C.K. Costello, Y.M. Wang, S.R. Bare, H.H. Kung, M.C. Kung, J. Catal. 210 (2002) 375.
[24] A. Wolf, F. Schüth, Appl. Catal. A: Gen. 226 (2002) 1.
[25] M. Manzoli, G. Avgouropoulos, T. Tabakova, J. Papavasiliou, T. Ioannides, F. Boccuzzi, Catal. Today 138 (2008) 239.
[26] A.C. Gluhoi, B.E. Nieuwenhuys, Catal. Today 122 (2007) 226.
[27] F. Arena, P. Famulari, G. Trunfio, G. Bonura, F. Frusteri, L. Spadaro, Appl. Catal. B: Environ. 66 (2006) 81.
[28] A. Tompos, M. Hegedűs, J.L. Margitfalvi, E.G. Szabó, L. Végvári, Appl. Catal. A: Gen. 334 (2008) 348.
[29] M. Haruta, N. Yamada, T. Kobyashi, J. Catal. 115 (1989) 301.
[30] H. Wang, J. Wang, W.-D. Xiao, W.-K. Yuan, Powder Technol. 111 (2000) 175.
[31] K.C. Song, Y. Kang, Mater. Lett. 42 (2000) 283.
[32] A. Tompos, J.L. Margitfalvi, E. Tfirst, L. Végvári, M.A. Jaloull, H.A. Khalfalla, M.M. Elgarni, Appl. Catal. A: Gen. 285 (2005) 65.
[33] Neal Fairley, 2006. <www.casaxps.com>.
[34] M. Mohai, XPS MultiQuant: Multi-model X-ray Photoelectron Spectroscopy Quantification Program, Version 3.00.16, 2003. <http://www.chemres.hu/aki/XMQpages/XMQhome.htm>.;
M. Mohai, Surf. Interface Anal. 36 (2004) 828.
[35] C.D. Wagner, A.V. Naumkin, A. Kraut-Vass, J.W. Allison, C.J. Powell, J.R. Rumble Jr., NIST X-ray Photoelectron Spectroscopy Database, Version 3.4, National Institute of Standards and Technology, Gaithersburg, MD, 2003. <http://srdata.nist.gov/xps/>.
[36] L. Vegard, Z. Phys. 5 (1921) 17.
[37] F. Khairallah, A. Glisenti, J. Mol. Catal. A 274 (2007) 137.
[38] S. Ardizzone, C.L. Bianchi, M. Fadoni, B. Vercelli, Appl. Surf. Sci. 119 (1997) 253.
[39] D.K. Aswala, K.P. Muthea, S. Tawdeb, S. Chodhuryb, N. Bagkarb, A. Singha, S.K. Guptaa, J.V. Yakhmia, J. Cryst. Growth 236 (2002) 661.
[40] P.H. Citrin, G.K. Wertheim, Phys. Rev. B 27 (1983) 3176.
[41] M.G. Mason, Phys. Rev. B. 27 (1983) 748.
[42] M. Manzoli, A. Chiorino, F. Boccuzzi, Surf. Sci. 532–535 (2003) 377.
[43] A. Simakov, I. Tuzovskaya, N. Bogdanchikova, A. Pestryakov, M. Avalos, M.H. Farias, E. Smolentseva, Catal. Commun. 9 (2008) 1277.
[44] E.Gy. Szabó, M. Hegedűs, F. Lónyi, Á. Szegedi, A.K. Datye, J.L. Margitfalvi, Catal. Commun. 10 (2009) 889.
[45] B.P. Barbero, L.E. Cadus, Appl. Catal. A: Gen. 234 (2002) 245.
[46] B.P. Barbero, L.E. Cadus, Appl. Catal. A: Gen. 244 (2003) 235.